Journal of Molecular Structure 1228 (2021) 129714

Contents lists available at ScienceDirect

Journal of Molecular Structure

journal homepage: www.elsevier.com/locate/molstr

Synthesis, X-ray, spectroscopy, molecular docking and DFT calculations of (*E*)-*N*'-(2,4-dichlorobenzylidene)-5-phenyl-*1H*-pyrazole-3-carbohydrazide

Khalid Karrouchi[a,*], Silvia A. Brandán[b,*], Mubashir Hassan[c], Khalid Bougrin[d,e], Smaail Radi[f], Marilena Ferbinteanu[g], Yann Garcia[h], M'hammed Ansar[i]

[a] *Laboratory of Analytical Chemistry and Bromatology, Faculty of Medicine and Pharmacy, Mohammed V University in Rabat, Morocco*
[b] *Cátedra de Química General, Instituto de Química Inorgánica, Facultad de Bioquímica, Química y Farmacia, Universidad Nacional de Tucumán, Ayacucho 471, 4000, Tucumán, Argentina*
[c] *Institute of Molecular Biology and Biotechnology/(IMBB), The University of Lahore, Lahore, 54000, Pakistan*
[d] *Equipe de Chimie des Plantes et de Synthèse Organique et Bioorganique, URAC23, Faculty of Science, B.P. 1014, Geophysics, Natural Patrimony and Green Chemistry (GEOPAC) Research Center, Mohammed V University in Rabat, Morocco*
[e] *Mohammed VI Polytechnic University, Lot 660, Hay Moulay Rachid, Benguerir, Morocco*
[f] *Laboratory of Applied Chemistry and Environment (LCAE), Department of Chemistry, Faculty of Sciences, University Mohamed Premier, Oujda 60000, Morocco*
[g] *Inorganic Chemistry Department, Faculty of Chemistry, University of Bucharest, Dumbrava Rosie 23, Bucharest 020462, Romania*
[h] *Institute of Condensed Matter and Nanosciences, Molecular Chemistry, Materials and Catalysis (IMCN/MOST), Université catholique de Louvain, Place L. Pasteur 1, 1348 Louvain-la-Neuve, Belgium*
[i] *Laboratory of Medicinal Chemistry, Faculty of Medicine and Pharmacy, Mohammed V University, Rabat, Morocco*

ARTICLE INFO

Article history:
Received 23 October 2020
Revised 29 November 2020
Accepted 30 November 2020
Available online 10 December 2020

Keywords:
Pyrazole
X-ray
DFT
NBO
AIM
Molecular docking

ABSTRACT

(*E*)-*N*'-(2,4-dichlorobenzylidene)-5-phenyl-*1H*-pyrazole-3-carbohydrazide (**E-DPPC**) has been synthesized and characterized by FT-IR, ^{1}H-NMR, ESI-MS, and single-crystal X-ray diffraction. The structures and properties of this new pyrazole-3-carbohydrazide derivative were studied in gas phase and aqueous solution by using Functional hybrid B3LYP/6-311++G** calculations in gas phase and in aqueous solution to study. Two stable structures (C1 and C2) with similar energies were found in the PES. C2 evidence a higher dipole moment and a volume contraction in solution attributed to the presence of donors and acceptors H bonds. Besides, the changes in orientation and direction of dipole moment vector in solution are attributed to the hydration of **E-DPPC** with water molecules. The repulsion existent between the negative MK, Mulliken and NPA charges on the N12 and O15 atoms explain the diminishing of N12-C14-O15 angle from 123.77 ° in gas phase to 123.03 ° in solution. Nucleophilic sites are visibly observed on the acceptor H bonds groups (N10, O15 and N22 atoms) while on the N18-H21, N12-H13, C11-H23, C2-H3, C17-H20 bonds characteristics electrophilic sites were found, being the N18-H21 bond the most labile donor of H bond with the lowest MEP and bond order values. NBO calculations suggest that C2 is clearly most stable in solution than in gas phase. AIM studies show that C2 is stable in both media due to new H bonds formed. Harmonic force fields in both media were calculated together with the scaled force constants while the 102 vibration normal modes expected for C2 were completely assigned. The comparisons of experimental NMR and UV-visible spectra with the corresponding predicted evidence reasonable correlations. Docking results also displayed that **E-DPPC** possessed good binding profile against receptor molecule and interacted with core residues of target protein.

1. Introduction

Pyrazole and similar heterocyclic compounds show bioactivity and have pharmacological properties [1]. Pyrazole derivatives have a wide range of biological activities, such as anti-cancer, antiviral, anti-tubercular, anti-inflammatory, analgesic, antioxidant, anti-diabetic, anti-alzheimer, antibacterial, antifungal and pestici-

* Corresponding authors.
E-mail addresses: khalid.karrouchi@um5s.net.ma (K. Karrouchi), brandansa@yahoo.com.ar (S.A. Brandán).

https://doi.org/10.1016/j.molstruc.2020.129714
0022-2860/

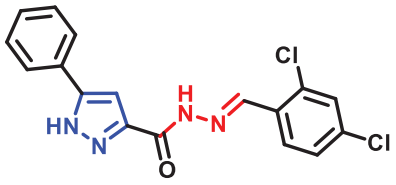

Fig. 1. Molecular structure of **E-DPPC**.

dal agents [2–14]. On the other hand, the carbohydrazides derivatives represent an important class of organic compounds in medicinal and pharmaceutical chemistry [15,16]. Various studies about the structural and vibrational analysis of compounds including pyrazole have been done [17–20]. In view of the therapeutic properties of these derivatives, the investigation of their molecular geometric structure, spectroscopic and electronic properties are fundamental to know the influence of different groups on structures in order to discover the relationship of these groups with their biological properties. In this context, DFT calculations have become a tool very reliable in predicting properties of molecules with great precision [21–27]. Due to the pharmacological importance of these classes of derivatives, in this work, (*E*)-*N*'-2,4-dichlorobenzylidene-5-phenyl-*1H*-pyrazole-3-carbohydrazide (**E-DPPC**) (Fig. 1) was synthesized and characterized by FT-IR, ^{1}H-NMR, EIS-MS spectrometry and single-crystal X-ray diffraction. The title compound has been analyzed from vibrational and theoretical point of view in order to study the structural, electronic and topological properties and, to perform the complete vibrational assignments. All these studies are very important to know the connections between the properties of this new pyrazole-3-carbohydrazide derivative with other reported from the literature [18,19].

Furthermore, natural bond orbital (NBO), atoms in molecules (AIM), and Frontier orbitals calculations were carried in gas phase and aaqueous solution in order to study the molecular geometric structure, bond orders, vibrational frequencies, ^{1}H-NMR chemical shifts, HOMO-LUMO and stabilization energies, atomic charges and molecular electrostatic potential (MEP) by using B3LYP method with the 6-311++G(d,p) basis set. At the same level of theory, the harmonic force field and the normal internal coordinates of **E-DPPC** were used to perform the complete assignments of all bands observed in the experimental FTIR spectrum by using the scaled quantum mechanical force field (SQMFF) methodology and the Molvib program [28,29]. Transferable scaling factors were also employed to obtain the main scaled force constants [30]. The properties here predicted for this new derivative were later compared with the reported for similar derivatives [18,19]. Comparisons of reactivity and behaviors of this new derivative were performed with other similar ones by using useful descriptors [18,19,22–26]. Furthermore, computational study was employed to check the binding potential of the synthesized compound. The best ligand (**E-DPPC**) was deeply analyzed to check its binding conformational position inside the active region of caspase-3.

2. Experimental section

2.1. General methods

All chemical reactions were purchased Sigma-Aldrich. Reactions were checked with TLC using aluminum sheets with silica gel 60 F254 from Merck. Melting points were measured using a Buchi B-545 digital capillary melting point apparatus and used without correction. The FT-IR spectrum was recorded with Perkin-Elmer VERTEX 70 FT-IR spectrometer covering field 400-4.000 cm^{-1}. ^{1}H-NMR spectra was recorded in solution in DMSO-d_6, on Bruker spectrometer (300 MHz). The chemical shifts are expressed in parts per million (ppm) by using tetramethylsilane (TMS) as internal reference. Mass spectra were collected using API 3200 LC/MS/MS system, equipped with an ESI source.

2.2. Synthesis

The title compound described here was facilely synthesized according to the literature procedures [31–34] (Scheme 1). To a solution of 5-phenyl-*1H*-pyrazole-3-carbohydrazide (**1**) (202 mg, 1 mmol) and 2,4-dichlorobenzaldehyde (**2**) (174 mg, 1 mmol) in ethanol (10 mL) was added two drops of acetic acid. The mixture was maintained under reflux for 2 h. Then, the precipitate formed was filtered and recrystallized from DMF/MeOH to give the pure product (**E-DPPC**).

White solid, Yield 62 %, M.p. 234-236°C; IR (ATR, ν(cm^{-1})): 3182 (NH), 1657 (C=O), 1586 (N=CH); ^{1}H-NMR (300 MHz, DMSO-d_6, δ(ppm)): 7.24 (s, 1H, H-pyrazole), 7.52-7.34 (m, 4H, H-Ar), 7.69 (d, J = 1.8 Hz, 2H, H-Ar), 7.82 (d, J = 7.5 Hz, 2H, H-Ar), 8.01 (d, J = 8.4 Hz, 2H, H-Ar), 8.89 (s, 1H, -CONH), 12.12 (s, 1H, N=CH) 13.83 (s, 1H, NH-pyrazole); MS: m/z = 359.0 [M+H]$^+$, 381.0 [M+Na]$^+$.

2.3. Single crystal X-ray diffraction

X-ray single crystal data were collected by using MoKα (λ = 0.71075 Å) radiation on a Rigaku R-Axis Rapid II diffractometer equipped with an large-area curved imaging plate detector (460.0 × 256.0 mm), 3-circle goniometer and high-frequency 5 kW sealed tube. All calculations were performed using the CrystalStructure [35] crystallographic software package except for refinement, which was performed using the software package Olex1.2 [36]. The structure was solved by direct methods and refined in a routine manner (SHELXL) [37]. Non-hydrogen atoms were refined anisotropically. Hydrogen atoms were refined using the riding model. Molecular graphics were generated by using MERCURY 3.9 [38] and POV-Ray software [39]. The details of the X-ray crystal data and the structure solution as well as the refinement are given in Table 1. A summary of selected bond lengths [Å] and angles [°] are given in **Table S1** (ESI). CCDC 2033972.

2.4. Computational details

The experimental CIF file determined by X-ray crystal data was used as initial theoretical structure of (*E*)-*N*'-2,4-dichlorobenzylidene-5-phenyl-*1H*-pyrazole-3-carbohydrazide (**E-DPPC**). The optimizations of **E-DPPC** were performed in gas phase and aqueous solution with the Revision A.02 of Gaussian 09 program by using the functional hybrid B3LYP/6-311++G** level of theory [40–42]. Studies of curves of potential energy surface (PES) to variations in the dihedral C16-C14-N12-N10 and N10-C11-C1-C2 angles by using the hybrid B3LYP/6-311++G** method in gas phase have evidenced two structures with minima and identical energies, named C1 and C2. The PES for the dihedral N10-C11-C1-C2 angle can be seen in **Fig. S1** of supporting material whiles the structures of C1 and C2 in **Fig. S2**. The atomic charges, bond orders, stabilization energies, molecular electrostatic potentials (MEP) were computed with the NBO, AIM programs and the Merz-Kollman scheme while the mapped MEP surfaces [43–46] were graphed with the *GaussView* program [47]. The gap values and chemical potential (μ), electronegativity (χ), global hardness (η), global softness (S), global electrophilicity index (ω) and global nucleophilicity index (E) descriptors calculations were computed with the frontier orbitals [18,19,22–26,48]. The SQMFF methodology, normal internal coordinates, scaling factors and the Molvib program were used to perform the complete vibrational assignments considering potential energy distribution (PED) contributions ≥ 10 % [28–30]. From known equations

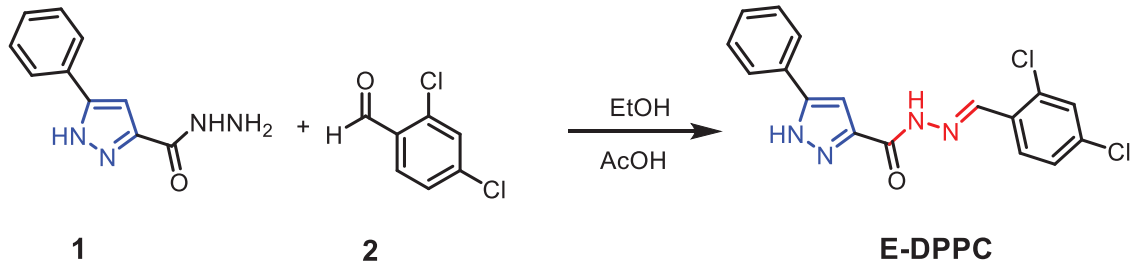

Scheme 1. The synthetic route for preparation of compound **E-DPPC**.

Table 1
Refinement parameters and crystal data for **E-DPPC.**

CCDC Deposition Number	CCDC 2033972
Empirical formula	$C_{37}H_{24}Cl_4N_9O_3$ {2($C_{17}H_{12}Cl_2N_4O$), 0.5($C_6N_2O_2$)}
Formula weight	784.472
Temperature/K	293.15
Crystal system	orthorhombic
Space group	*Pbcn*
a/Å	10.6297(4)
b/Å	14.1275(6)
c/Å	25.2639(17)
α/°	90
β/°	90
γ/°	90
Volume/Å^3	3793.9(3)
Z	4
ρ_{calc}g/cm^3	1.373
μ/mm^{-1}	0.361
F(000)	1607
Crystal size/mm^3	0.7 × 0.25 × 0.2
Radiation	Mo Kα (λ = 0.71075)
2Θ range for data collection/°	5.98 to 54.96
Index ranges	-13 ≤ h ≤ 13, -18 ≤ k ≤ 16, -32 ≤ l ≤ 32
Reflections collected	23424
Independent reflections	4344 [R_{int} = 0.0601, R_{sigma} = 0.0417]
Data/restraints/parameters	4344/0/254
Goodness-of-fit on F^2	1.089
Final R indexes [I>=2σ (I)]	R_1 = 0.0556, wR_2 = 0.1534
Final R indexes [all data]	R_1 = 0.1018, wR_2 = 0.1880
Largest diff. peak/hole / e Å^{-3}	0.34/-0.42

the Raman spectra predicted in activities were transformed to intensities [49,50]. The ultraviolet-visible and ^{1}H and ^{13}C NMR spectra in aqueous solution were also predicted at the same level of theory with time-dependent DFT calculations (TD-DFT) and the GIAO method [51]. The self-consistent reaction field (SCRF) and the integral equation formalism variant polarised continuum model (IEFPCM) methods were used together with universal solvation model to calculate the properties in aqueous solution [52–54] while the volumes in both media were computed with the Moldraw program [55].

2.5. In silico *Methodology*

2.5.1. *Retrieval of caspase-3 structure from PDB*

The three dimensional (3D) structure of caspase-3 from human was accessed from Protein Data Bank (PDB) (www.rcsb.org) having PDBID 2XYG. The selected target protein structure was minimized by using UCSF Chimera 1.10.1 tool [56] to further utilize it in docking experiment. Ramachandran and Hydrophobicity (**Figs S3** and S**4**) plots of caspase-3 were accessed from Discovery Studio 4.1 Client tool [57].

2.5.2. *Designing of ligands and Molecular docking*

The synthesized ligand (**E-DPPC**) was sketched in drawing ACD/ChemSketch tool and minimized by UCSF Chimera 1.10.1. The energy minimization was performed using default parameters, steepest descent steps 100 with step size 0.02 (Å), conjugate gradient steps 100 with step size 0.02 (Å) and update interval was fixed at 10. Molecular docking experiment was employed between **E-DPPC** against caspase-3 using PyRx virtual screening tool with AutoDock VINA Wizard approach [58]. The grid box center values of (center_X = 29.43, Y = 21.31 and Z = 38.34) and size values were adjusted as (X = 44.02, Y = 55.00 and Z = 39.718908395) for better conformational position in the active region of target protein. The default exhaustiveness value = 8 was used in docking experiment. The predicted docked complexes were evaluated on the basis of lowest binding energy (Kcal/mol) values and structure activity relationship (SAR) analyses. The three dimensional (3D) graphical depictions of all the docked complexes were accomplished by Discovery Studio (2.1.0) and UCSF Chimera 1.10.1 tool.

3. Results and discussion

3.1. *X-ray crystal structure description*

The compound (**E-DPPC)** was analysed by single crystal X-ray diffraction. The summary of crystallographic information is listed in Table 1. The compound (**E-DPPC)** crystalized in the orthorhombic, space group *Pbcn*. The crystal structure shows a cvasi-planar structure (Fig. 2 **and S5**). The molecule has the carbonylic O atom located in an anti-position with pyrazolic N atoms. If we consider the carbohydrazide fragment as a reference plan, it can be observe

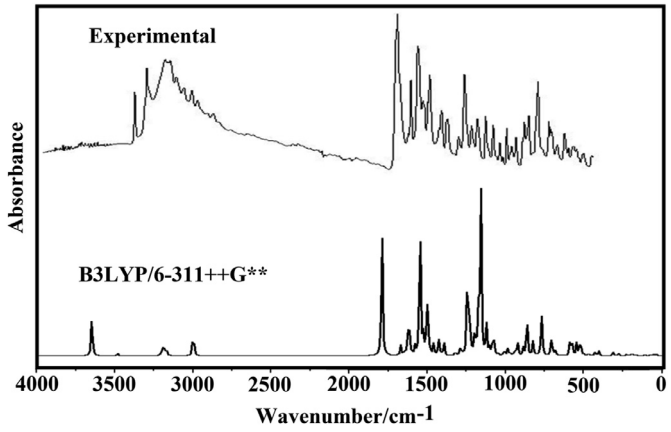

Fig. 2. X-ray molecular structure of compound **E-DPPC** with atoms numbering scheme. Thermal ellipsoids representation with 50% probability. Olex and POV-Ray representation. Solvent molecules are omitted for clarity.

Table 2
Calculated total energies (*E*), dipole moments (μ) and volumes (V) of (*E*)-*N*'-2,4-dichlorobenzylidene-5-phenyl-*1H*-pyrazole-3-carbohydrazide (E-DPPC) in gas phase and aqueous solution by using the hybrid B3LYP/6-311++G** Method.

B3LYP/6-311++G** Method					
Medium C2	E (Hartrees)	ZPVE (Hartrees)	μ (D)	V (Å^3)	ΔV (Å^3)
GAS	-1869.9171	-1869.6566	8.85	342.8	-
PCM/Water	-1869.9567	-1869.6535	14.03	342.6	0.2

that pyrazolic fragment is tilted with 11.30º, since the dichlorobenzylidene fragment make an angle of 17.13º with the reference plan. The molecules are arranged two by two in a zig-zag fashion in a very compact packing (**Fig. S6**). The crystal contain DMF solvent molecule which are disordered over two positions. However, the disordered solvent molecule does not affect the compound structure, but slightly affect the structure parameters.

3.2. Optimizations in both media

B3LYP/6-311++G** calculations have optimized the structures of two C1 and C2 conformers of **E-DPPC** with the same energy values, as observed in PES from **Fig. S1**. Hence, in this work only uncorrected and corrected calculated total energy, dipole moments and volumes for C2 of E-DPPC in gas phase and aqueous solution are presented in Table 2.

The results for this conformer evidence a higher dipole moment value and a volume contraction in solution with a difference in the volume of -0.2 Å^3. The presence of two donors H bonds groups (N-H) and of five acceptors H bonds (N and O atoms) justify the hydration of **E-DPPC** in solution and the increases of dipole moment in this medium. It is very interesting to observe from **Fig. S7** that the orientation and direction of dipole moment vector for C2 of **E-DPPC** in gas phase by using the B3LYP/6-311++G** level of theory is slightly different from that observed in solution. The changes in orientation and direction of dipole moment vector in solution are attributed to the hydration of **E-DPPC** with water molecules. On the other hand, the calculation of corrected solvation energy of **E-DPPC** in aqueous solution is presented in Table 3 together with the predicted for (*E*)-*N*'-4-methoxybenzylidene)-5-methyl-1H-pyrazole-3-carbohydrazide (**E-MBPC**) (-131.34 kJ/mol) and (*E*)-*N*'-(4-(dimethylamino)benzylidene)-5-methyl-*1H*-pyrazole-3-carbohydrazide (**E-MABPC**) (-129.50 kJ/mol) derivatives [18,19]. The results have shown a ΔG_c value of -130.83 kJ/mol.

This value is between those observed for **E-MBPC** (-131.34 kJ/mol) and **E-MABPC** (-129.50 kJ/mol) [18,19]. Structures of three

Table 3
Corrected and uncorrected solvation energies by the total non-electrostatic terms and by zero point vibrational energy (ZPVE) (*E*)-*N*'-4-methoxybenzylidene)-5-methyl-1H-pyrazole-3-carbohydrazide (E-MBPC) in aqueous solution by using the B3LYP/6-311++G** Method.

B3LYP/6-311++G** method[a]			
Solvation energy (kJ/mol)			
Species	$\Delta G_{un}{}^{\#}$	ΔG_{ne}	ΔG_c
E-DPPC[a]	-103.87	26.96	-130.83
E-MBPC[b]	-103.08	28.26	-131.34
E-MABPC[c]	-105.97	23.53	-129.50

$\Delta G_{un}{}^{\#}$= uncorrected solvation energy; ΔG_{ne}= total non electrostatic terms; ΔG_c= corrected solvation energies.
[a] This work
[b] From Ref [18] for (E-MBPC) (*E*)-*N*'-4-methoxybenzylidene)-5-methyl-1H-pyrazole-3-carbohydrazideFrom Ref [19] for (E-MABPC) (*E*)-*N*'-(4-(dimethylamino)benzylidene)-5-methyl-*1H*-pyrazole-3-carbohydrazide

compared compounds can be seen in **Fig. S8**. Note that the higher ΔG_c value observed for E-MBPC could be associated to the presence of $N(CH_3)_2$ group acceptor of H bonds in solution while the presence of two phenyl rings in **E-DPPC** where one of them has two deactivate Cl atoms produce decreasing in the ΔG_c value.

Comparisons of geometrical parameters calculated for C2 of **E-DPPC** in both media by using B3LYP/6-311++G** calculations with the corresponding experimental ones determined here are summarized in **Table S1** together with the root-mean-square deviation (RMSD) values. Better RMSD correlations for C2 of **E-DPPC** in both media are observed in the bond lengths than the bond angles, with values between 0.020 and 0.017 Å for distances and 2.406 and 2.401 ° for angles. The hydration in aqueous solution produce lengthening of O15-C14 and N10-N12 bonds while the C16-C14 bond undergoes decreases in the same medium. On the other hand, the C19-N18-N22, C14-N12-N10, N12-C14-O15 and C16-C14-O15 angles involved in those bonds also undergo changes as a consequence of hydration in those regions by water molecules.

3.3. Atomic charges, molecular electrostatic potentials and bond orders

Atomic charges such as, Merz-Kollman (MK), Mulliken and natural population (NPA) charges are very important parameters to explain the behaviours of species in different medium and specifically in solution [43,46]. In addition, in species with acceptors and donors H bonds groups, as in C2 of **E-DPPC**, the molecular electrostatic potentials (MEP) and bond orders (BO) are properties that describe the nucleophilic and electrophilic sites where the reactions with potential electrophils and nucleophils take place and also, reveal witch the most labile groups are. For these reasons, in **Table S2** those three atomic charges, molecular electrostatic potentials (MEP) and bond orders calculated for C2 of **E-DPPC** in both media by using the B3LYP/6-311++G** method are presented. If the atomic charges are analyzed only on the N10, N12, H13,C14, O15, N18 and N22 atoms belonging to acceptors and donors H bonds groups from **Fig. S9** it is observed that the behaviours of atomic charges are different among them. However, the variation of each atomic charge is the same in both media. Hence, (i) the MK and NPA charges on N10 have negative signs in both media while the Mulliken charges show positive signs in both media, (ii) the three charges on N12 and O15 have negative signs while on the H13 and H21 positive signs, (iii) the MK and NPA charges on C14 have positive signs in both media while the Mulliken charges show negative signs and finally, (iv) the Mulliken charges on N22 present positive values in both media while the MK and NPA charges have negative signs. Therefore, the diminishing of N12-C14-O15 angle from 123.77 ° in gas phase to 123.03 ° cannot be explained by the

three types of charges however, explain strongly the diminishing of C16-C14-O15 angle from 124.24 ° in gas phase to 122.71 ° in solution due to the repulsion existent between the negative MK, Mulliken and NPA charges on the N12 and O15 atoms.

The molecular electrostatic potentials (MEP) values on all atoms of C2 of **E-DPPC** in both media have been calculated from the MK charges and they are presented in Table S2 [46]. The MEP values show the following trend in both media: Cl > O > N > C > H, where the most negative values are observed on the Cl atoms while the less negative on the H atoms. Besides, the MEP values in general decrease in solution. If now the MEP values are analyzed only on the N10, N12, H13, C14, O15, N18 and N22 atoms belonging to acceptors and donors H bonds groups it is observed practically the same values and behaviours in both media and, in particular, on N10 and O15 are observed the higher negative values and on the H13 and H21 atoms the less negative values. Clearly, the N10 and O15 atoms belong to N10=C11 and C14=O15 bonds, respectively and, for these reasons, they have double bond characters with higher MEP values. On the other side, the H21 atoms (-0.974/-0.972 a.u.) present lower values in both media than the corresponding to H13 ones (-0.996/-0.981 a.u.) indicating that those N18-H21 bonds are most labile than the N12-H13 ones. The mapped surface for C2 of **E-DPPC** in gas phase is graphed with the *GaussView* program and, it is presented in **Fig. S10** [47]. The different colorations describe the nucleophilic and electrophilic sites where the reactions with potential electrophils and nucleophils can occur and also reveal witch the most labile groups are. The strong red colours are visibly observed on the acceptor H bonds groups which are the N10, O15 and N22 atoms and, hence, these red and orange regions are nucleophilic sites. Also, on a region of Cl24 a soft orange colour it is observed. On the contrary, on the aromatic N-H and C-H bonds and, in particular the N18-H21, N12-H13, C11-H23, C2-H3, C17-H20 bonds blue colours are observed. These blue sites are electrophilic places and are characteristics of donors H bonds groups. Note that the strong blue colour is observed on the N18-H21 bond because this group is the most labile donor of H bond with the lowest MEP value.

Bond orders (BO), expressed as Wiberg index, were also studied for C2 of **E-DPPC** in both media by using the B3LYP/6-311++G** method. These parameters were calculated from the NBO calculations [43]. The obtained results are presented in Table S2. The analyses reveal that the C6 and C9 atoms linked to Cl25 and Cl24 atoms, respectively present the higher BO values (4.018/4.024) in both media than the other ones while the N18 atoms belonging to N18-H21 bonds have the higher values (3.479/3.483) than the N10, N12 and N22 atoms and, for these reasons, the H21 atoms linked to N18 are the most labile and with low BO values in both media (0.839). Studies performed in this section by using atomic charges, MEP and BOs suggest that the N10, O15 and N22 atoms are the higher acceptors of H bonds in solution while the N18-H21 is the most important donor H bonds in the same medium.

3.4. NBO and AIM studies

NBO calculations by using the NBO 3.1 program allows the determination of many properties such as those previously studied atomic NPA charges and bonds orders. Other interesting property to explore with that program is the donor-acceptor energy interaction by using Second Order Perturbation Theory Analysis of Fock Matrix in NBO Basis [43]. Hence, the energy E(2) calculated as the difference between the donor NBO j and the acceptor NBO i, that is, E(j)-E(i) result the donor-acceptor energy interaction or delocalization energy. Therefore, for the conformer C2 of **E-DPPC** in gas phase and aqueous solution main delocalization energies by using the hybrid B3LYP/6-311++G** method can be seen in **Table S3**. Regarding the results, five different interactions are predicted for C2 in the two media which are, the $\Delta E_{\pi\rightarrow\pi^*}$, $\Delta E_{n\rightarrow\pi^*}$, $\Delta E_{n\rightarrow\sigma^*}$, $\Delta E_{\pi^*\rightarrow\pi^*}$ and $\Delta E_{\pi^*\rightarrow\sigma^*}$ interactions where the higher energy values are observed for $\Delta E_{\pi\rightarrow\pi^*}$ (1361.97/1356.20 kJ/mol) and $E_{\pi^*\rightarrow\pi^*}$ (2203.11/2632.48 kJ/mol) interactions in both media. The number of interactions are related to the charges transfer from π orbitals of two phenyl and pyrazole rings to π antibonding orbitals of two phenyl and pyrazole rings, as detailed in Table S2. Note that the charges transfer from lone pairs of N12, O15, N18, Cl24 and Cl25 atoms to antibonding orbitals of pyrazole ring and carbohydrazide group ($\Delta E_{n\rightarrow\pi^*}$ and $\Delta E_{n\rightarrow\sigma^*}$) present lower energy values, as compared with other observed interactions. Hence, the total energy value favour to **E-DPPC** in solution probably due to the hydration. Hence, C2 in aqueous solution is clearly most stable than in gas phase.

The topological properties calculated by using the Bader's theory of atoms in molecules (AIM) with the AIM 2000 program are useful parameters to search different intra-molecular or H bonds interactions in the conformer C2 of **E-DPPC** in both media. Hence, in **Table S4** are presented the electron density distribution, $\rho(r)$, the Laplacian values, $\nabla^2\rho(r)$, the eigenvalues ($\lambda 1$, $\lambda 2$, $\lambda 3$) of the Hessian matrix and the $\lambda 1/\lambda 3$ ratio in the Bond Critical Points (BCPs) and Ring critical point (RCPs) for C2 of **E-DPPC** in gas phase and aqueous solution by using the hybrid B3LYP/6-311++G** Method. From the analysis it is possible to observe the formation of a new H bonds in both media, that is, the C11-N10•••Cl24 interaction. This new H bond interaction can be seen in the molecular graphic of conformer C2 of **E-DPPC** in gas phase presented in **Fig. S11**. As a consequence of those new C11-N10•••Cl24 interactions new RCPs appear named RCPN1 while the RCP own of each ring are named RCP1, RCP2 and RCP3. RCP1 corresponds to phenyl ring, RCP2 corresponds to pyrazole ring and RCP3 corresponds to dichlorobenzylidene ring (See Fig. S8). The distance between the involved N10 and Cl24 atoms is shorter in gas phase than in aqueous solution while the topological properties of pyrazole rings in both media are higher than the other ones. This study shows that C2 of **E-DPPC** is stable in both media due to new H bonds formed.

3.5. Frontier orbitals and global descriptors

To known if this new synthetized pyrazole-3-carbohydrazide (**E-DPPC**) derivative is important from a pharmacological point of view [3,5,9,10,15,16,18] the energy gap and various descriptors are valuable parameters to predict reactivity and behaviour of many species in different media [22–26,48]. Hence, for conformer C2 of **E-DPPC** in gas phase and aqueous solution have been computed the HOMO, LUMO, Gap and the chemical potential (μ), electronegativity (χ), global hardness (η), global softness (S), global electrophilicity index (ω) and nucleophilicity indexes (E) descriptors by using the frontier orbitals and the hybrid B3LYP/6-311++G** method. The results for C2 are presented in **Table S5** compared with the reported for (*E*)-*N*'-4-methoxybenzylidene)-5-methyl-*1H*-pyrazole-3-carbohydrazide (**E-MBPC**) and (*E*)-*N*'-(4-(dimethylamino)benzylidene)-5-methyl-*1H*-pyrazole-3-carbohydrazide (E-MABPC) derivatives [18,19]. The structures of compared compounds can be seen in **Fig. S8**. The evaluation of gap values in both media shows that C2 in solution (4.3294 eV) has a lower value than that observed in gas phase (4.3674 eV) indicating this way, that C2 is most reactive in solution. Gap's values comparisons with the other two derivatives evidence a higher reactivity of E-MABPC, due to its low gap value, while C2 of **E-DPPC** in both media are less reactive than other ones. The presence of O-CH_3 group containing a strong acceptor of H bonds in E-MABPC probably justify its higher reactivity while the two deactivating Cl atoms in the phenyl ring together a other phenyl ring linked to pyrazole ring in E-MABPC generate lower reactivities

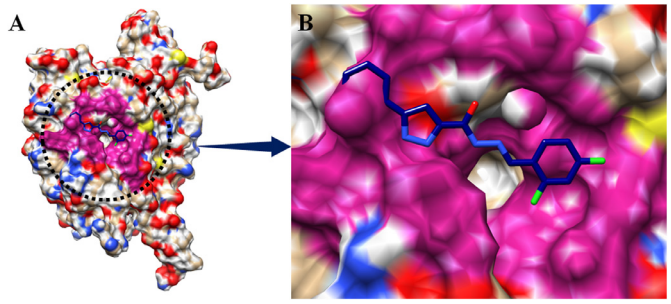

Fig. 3. Experimental FT-IR spectrum of **E-DPPC** in the solid state using reflectance (ATR) mode compared with the corresponding predicted for the most stable conformer C2 in the gas phase by using the B3LYP/6-311++G** method.

in both media. This higher reactivity in E-MABPC is in agreement with the lower solvation energy predicted in aqueous solution for E-MABPC (-129.50 kJ/mol), as was studied in section 3.2. In relation to the descriptors, obviously, the most reactive E-MABPC has the higher global hardness (η) and lower global softness (S), as expected but probably, the lower global electrophilicity (ω) and nucleophilicity indexes (E) could justify its high reactivity, as compared with E-MBPC and **E-DPPC**.

3.6. Vibrational study

The experimental FT-IR spectrum of E-DPPC was recorded in the solid state using reflectance (ATR) mode and it can be observed in Fig. 3 compared with the corresponding predicted for the most stable conformer C2 in the gas phase by using the B3LYP/6-311++G** method. The predicted Raman spectrum of C2 in activities at the same level of theory was corrected to intensities by using recommended equations and, it is given in **Fig. S12** [49,50]. The C2 conformer of **E-DPPC** in both media was optimized at the same level of theory with C_1 symmetries and, due to the 36 atoms present in its structure, 102 vibration normal modes are expected. Hence, all vibration modes have activity in the infrared and Raman spectra. The scaled quantum mechanical force field (SQMFF) methodology and the Molvib program were used in the determination of harmonic force fields of C2 in both media together with the normal internal coordinates and transferable scaling factors [28–30]. In the vibrational analysis only potential energy distribution (PED) contributions $\geq$ 10 % were employed. In Table 4 are summarized experimental and calculated wavenumbers for C2 in gas phase by using B3LYP/6-311++G** calculations. Below, a brief discussion of assignments by regions is presented.

3.6.1. Bands assignments

4000-2000 cm^{-1} region. This region is typical of N-H and C-H stretching modes. The NH group are very characteristic and their stretching vibrations are generally observed around 3500–3300 cm^{-1} [18,19,22–27]. The NH stretching vibrations for pyrazole are reported at 3232 and 3322 cm^{-1} for (*E*)-*N*'-(4-(dimethylamino)benzylidene)-5-methyl-*1H*-pyrazole-3-carbohydrazide (**2**) and (*E*)-*N*'-(4-methoxybenzylidene)-5-methyl-*1H*-pyrazole-3-carbohydrazide (**E-MBPC**), respectively [18,19]. In this study, the bands appear at 3400 cm^{-1} and 3324 cm^{-1} have been assigned to N-H stretching modes of vibrations for pyrazole and hydrazonoic group, respectively.

The C-H stretching vibrations of aromatic rings give rise to bands in the region 3200-3000 cm^{-1} in aromatic compounds [18–20,22–27]. For **E-DPPC**, a series of infrared absorptions between 3204 and 2888 cm^{-1} were assigned as CH stretching modes, the band at 3204 cm^{-1} is assigned as C-H stretching vibrations in the pyrazole ring, which is in good agreement with the values reported for pyrazole derivatives [18–20]. The absorption bands which appear between 3169, 3132, 3079, 3027, 2990, 2925 and 2888 cm^{-1} have been assigned as CH stretching modes of hydrazonoic group, phenyl and 2,4-dichlorobenzyl rings, as detailed in Table 4.

2000-1000 cm^{-1} region. In this region are expected the C=O, C=C, C-C and C-N stretching modes, deformation and rocking modes of NH, CH groups and, some deformations of pyrazole and benzyl rings can also be observed. The C=O stretching absorption is usually one of the most representative in an infrared spectrum, it appears in a wavenumber region relatively free of other vibrations (1800-1600 cm^{-1}) [18–20]. For this molecule, $\nu_{C=O}$ vibration originates one of the strongest bands of the infrared spectrum, at 1683 cm^{-1}. The aromatic C=C stretching vibrations are very much important and occur in the region 1650-1200 cm^{-1} [18–20,22–27]. For **E-DPPC**, the bands observed at 1593 and 1547 cm^{-1} were assigned to C=C stretching vibrations in phenyl, 2,4-dichlorobenzyl and pyrazole rings. The bands observed at 1593 and 1547 cm^{-1} are also assigned to C=N stretching mode of pyrazole and hydrazonoic group, respectively, and some IR bands of media intensities observed at 1386 and 1352 cm^{-1} are assigned to C-C and C-N stretching modes. Other C-C stretching modes are associated to the bands observed at 1281, 1241 and 1098 cm^{-1}.

The N–N vibration modes corresponding to pyrazole and hydrazonoic group are reported at 1106 and 1121 cm^{-1}, respectively [20]. For **E-DPPC**, these N18-N22 and N10-N12 stretching modes are assigned respectively to the strong bands at 1195 and 1101 cm^{-1}.

The NH in-plane deformation vibration is reported at 1509 and 1210 cm^{-1} in pyrazole and hydrazonoic group, respectively [20]. In this derivative, the SQM calculations have predicted the N12-H13 and N18-H21 in-plane deformation vibrations at 1505 and 1418 cm^{-1} and, hence, the IR bands observed at 1509 and 1386 cm^{-1} are assigned to those vibration modes of hydrazonoic group and pyrazole, respectively. Here, it is very important to mention that the SQM calculations predict the N12-H13 in-plane deformation mode with an intensity higher than the C=O stretching mode, as observed in Table 4. This observation is very interesting taking into account that the N12-H13 is less labile than the other N18-H21 one. The C-H in-plane deformation vibrations are observed in the region 1300–1000 cm^{-1} and are usually of medium to weak intensity [18–20,22–27]. Here, some bands due to C–H in-plane bending vibration in both species interact somewhat with other vibrations and they can be assigned to the bands in the region between 1467 and 1061 cm^{-1}.

1000-400 cm^{-1} region. In this region, the C-C and C-N stretching modes, C-H and N-H out-of-plane deformations, deformations, wagging and twisting modes of C=O group, twisting CH_3 and deformations and torsions modes of pyrazole, phenyl and 2,4-dichlorobenzyl rings are expected. In the (*E*)-*N*'-(4-methoxybenzylidene)-5-methyl-1H-pyrazole-3-carbohydrazide derivative, the C=O in-plane and out-of-plane deformations are assigned to 897 and 760 cm^{-1}, respectively [20]. Hence, the IR bands observed at 905 and 757 cm^{-1} are assigned to those vibration modes.

The out-of-plane CH deformations are predicted and assigned between 1100 and 600 cm^{-1} [18–20,22–27]. In this molecule, the IR bands between 995 and 757 cm^{-1} are assigned to those vibration modes. The other skeletal vibrations are assigned as predicted by the SQM calculations and, in according assignments for similar groups [18–20,22–27].

3.7. Force fields

Scaled internal force constants are interesting parameters that describe the forces of different bonds and they can be compared with values reported for similar derivatives in order to

Table 4
Observed and calculated wavenumbers (cm^{-1}) and assignments for (*E*)-*N'*-2,4-dichlorobenzylidene-5-phenyl-*1H*-pyrazole-3-carbohydrazide (**E-DPPC**) in gas phase by using the hybrid B3LYP/6-311++G** Method.

Exp[a]	B3LYP/6-311++G** method[a]			
IR	Calc[b]	Int[c]	SQM[d]	Assignments[a]
3400m	3646	104.4	3495	νN18-H21
3324s	3478	4.4	3334	νN12-H13
3204s	3251	0.2	3117	νC17-H20
3169s	3216	0.7	3083	νC7-H8
3132s	3209	1.3	3076	νC4-H5
3079m	3195	10.9	3063	νC33-H36
3079m	3186	18.7	3055	νC28-H32,νC29-H34
3027m	3179	8.6	3047	νC33-H36,νC28-H32
3027m	3170	0.1	3039	νC31-H35
2990m	3169	7.5	3038	νC2-H3
2925w	3163	5.8	3032	νC27-H30
2888w	2997	58.9	2872	νC11-H23
1683vs	1788	319.3	1723	νC14=O15
1593s	1668	20.6	1609	νC11=N10
1593s	1645	8.0	1592	νC27-C29
1593s	1619	96.7	1567	νC29-C33
1547s	1618	17.8	1566	νC2-C4
1547s	1598	2.3	1545	νC17-C19
1547s	1578	18.1	1526	νC4-C6
1509m	1546	375.3	1505	βN12-H13
1467m	1523	49.4	1477	βC31-H35
1467m	1500	140.3	1454	βC2-H3,βC7-H8
1445sh	1485	13.2	1442	βC33-H36,βC29-H34
1386m	1460	25.9	1418	βN18-H21,νC14-C16
1386m	1431	10.8	1389	νC16-N22
1386m	1425	28.9	1378	νC16-C17,νC19-N18
1361sh	1411	3.3	1369	βC11-H23
1352m	1392	31.3	1352	νC7-C9
1324sh	1356	0.3	1318	βC28-H32,βC27-H30
1281w	1328	3.4	1283	νC28-C26
1281w	1320	4.5	1273	νC9-C1,νC6-C7
1241s	1288	15.7	1244	νC27-C26
1241s	1278	6.6	1243	βC7-H8
1241s	1243	176.7	1202	νC1-C11,νC1-C2
1195m	1232	126.7	1192	νN18-N22
1167sh	1207	2.0	1172	βC29-H34
1155m	1197	63.0	1162	βC17-H20
	1185	0.6	1152	βC33-H36
1143sh	1175	100.2	1141	βC4-H5
1101s	1158	437.7	1120	νN10-N12
1101s	1121	68.9	1084	νC6-Cl25,βR_1(A3)
1098s	1103	6.9	1067	νC28-C31
1061sh	1099	15.5	1065	νN10-N12,βC17-H20
1052m	1082	20.8	1054	βR_1(A3)
1042m	1073	29.3	1045	νC14-N12
1016w	1050	3.6	1018	νC31-C33
1005m	1015	1.4	999	βR_1(A1)
995vw	1007	13.1	996	γC33-H36
985vw	1004	0.1	985	βR_2(A2)
969s	984	6.8	974	γC29-H34,γC31-H35
962s	983	9.7	963	βR_1(A2)
957sh	965	5.7	957	γC2-H3
930w	943	8.9	936	γC11-H23
	929	1.4	919	γC27-H30,γC28-H32
905m	924	33.8	911	βC14=O15
870sh	886	16.6	878	γC7-H8
849s	862	105.9	847	βR_3(A3)
842sh	853	0.3	842	γC27-H30,γC28-H32
828sh	822	22.0	812	γC4-H5
788sh	820	10.6	810	γC17-H20
757vs	779	6.4	767	γC14=O15
757vs	770	82.1	759	γC14=O15,γC17-H20
747sh	763	16.7	748	βR_3(A3)
687s	716	0.1	695	τR_1(A3),γC1-C11
687s	707	32.6	692	βR_3(A1)
687s	702	4.8	688	τR_1(A1)
680sh	696	9.3	679	τR_2(A2),γC19-C26
676sh	685	2.7	675	βR_2(A3)
662sh	677	9.5	662	τR_1(A2)
631m	633	0.7	629	βR_2(A1)
585s	586	36.0	578	γN18-H21
573sh	579	7.7	566	τR_2(A3), γC6-Cl25

(*continued on next page*)

Table 4 (*continued*)

Exp[a]	B3LYP/6-311++G** method[a]			
IR	Calc[b]	Int[c]	SQM[d]	Assignments[a]
558m	570	20.9	559	βC1-C11
526m	543	26.3	536	γN12-H13,τR_2(A1)
505m	522	43.0	516	γN12-H13
492sh	499	2.6	490	γC26-C19
459w	469	3.8	459	τR_3(A3)
450sh	461	1.7	450	τR_3(A3), γC9-Cl24
420sh	426	6.0	419	βC26-C19
414sh	421	2.4	412	βR_3(A3), νC9-Cl24
406w	411	0.0	398	τR_3(A1)
	400	10.3	390	νC6-Cl25,νC9-Cl24
	389	0.5	368	τN10-C11
	349	0.0	346	βC9-Cl24,βC6-Cl25
	312	8.9	305	τR_2(A1)
	286	1.7	280	νC19-C26
	273	4.9	260	τN12-C14,βC14-C16
	226	4.3	219	τR_2(A1), βC14-C16
	208	0.6	207	C9-Cl24,βC6-Cl25
	196	3.0	192	γC16-C14
	185	0.6	179	βC6-Cl25,τN10-C11
	181	2.8	172	τR_3(A3), τR_2(A3)
	160	3.1	153	τN10-N12,γC6-Cl25
	113	1.2	111	βC19-C26
	104	0.8	98	τN10-N12,γN12-H13
	79	0.9	75	τN10-N12
	65	1.6	64	δC1C11N10,βC14-C16
	50	2.9	46	τ_wC26-C19
	32	3.0	30	τC14-C16
	24	0.3	23	δC16C14N12,δC14N12N10,δC11N10N12
	19	0.1	17	τN12-C14
	14	0.0	12	τC11-C1

Abbreviations: ν, stretching; β, deformation in the plane; γ, deformation out of plane; wag, wagging; τ, torsion; β_R, deformation ring τ_R, torsion ring; ρ, rocking; τw, twisting; δ, deformation; a, antisymmetric; s, symmetric; (A_1), Ring 1; (A_2), Ring 2; (A_3), Ring 3

[a] This work

[b] From B3LYP/6-311++G** method

[c] Intensities in KM/Mole

[d] From scaled quantum mechanics force field.

explain some differences among their properties [18,19]. Here, the scaled internal force constants for C2 of **E-DPPC** in both media by using B3LYP/6-311++G** calculation were calculated from the harmonic force fields transformed from Cartesian coordinates to normal internal coordinates with the SQMFF methodology and the Molvib program [28–30]. The results are presented in Table 5 compared with the reported for (*E*)-*N*'-4-methoxybenzylidene)-5-methyl-*1H*-pyrazole-3-carbohydrazide (E-MBPC) and (*E*)-*N*'-(4-(dimethylamino)benzylidene)-5-methyl-*1H*-pyrazole-3-carbohydrazide (E-MABPC) [18,19].

Analyzing the values for C2 of **E-DPPC** in both media it is observed important differences in aqueous solution as compared with the values in gas phase. Hence, the $f(\nu N\text{-}H)$, $f(\nu C\text{-}H)_{R1}$, $f(\nu C{=}O)$, $f(\nu C\text{-}N)_R$, $f(\nu N\text{-}N)_{Chain}$ and $f(\nu C{=}C)_{R2}$ force constants are modified in solution due to the hydration. Only, the $f(\nu C\text{-}N)_{Chain}$ and $f(\nu C{=}C)_{R2}$ force constants increase its values while the other ones decrease, as a consequence of hydration. These modifications in the force constants values indicate clearly that the acceptors (N and O) and donors (N-H) H bonds groups are principally hydrated in solution. Note that the changes in the values related to pyrazole ring produce changes in $f(\nu C{=}C)_{R1}$ and $f(\nu C{=}C)_{R2}$ force constants but no in $f(\nu C{=}C)_{R3}$ force constant. Then, the deactivating Cl atoms in dichlorobenzylidene ring do not modify the properties of **E-DPPC** in solution. When the values of **E-DPPC** are compared with the corresponding to E-MBPC and E-MABPC changes in the force constants related to part common, pyrazole ring and carbohydrazide group, among the three structures are observed (see Figure S8). Hence, the differences among the $f(\nu C{=}O)$, $f(\nu N\text{-}N)_{Chain}$ and $f(\nu C\text{-}N)_{Chain}$ force constants in the three compounds are attributed to the groups linked to pyrazole ring and to the carbohydrazide group. Evidently, $f(\nu C\text{-}N)_{Chain}$ force constant in E-MBPC is higher than the other ones due to that the carbohydrazide group in this species is linked to phenyl ring and to $N(CH_3)_2$ group while in E-MABPC that groups is linked to phenyl ring and to O-(CH_3) group.

Table 5
Scaled internal force constants for (*E*)-*N*'-2,4-dichlorobenzylidene-5-phenyl-*1H*-pyrazole-3-carbohydrazide (**E-DPPC**) in gas and aqueous solution by using the B3LYP/6-311++G** method.

Force constants	**E-DPPC**[a]		**E-MBPC**[b]		**E-MABPC**[c]	
	Gas	PCM	Gas	PCM	Gas Phase	
					Free base	Cationic
$f(\nu N\text{-}H)$	6.47	6.39	6.50	6.45	6.49	5.72
$f(\nu C{=}O)$	11.92	9.97	11.76	9.62	11.69	9.15
$f(\nu C\text{-}H)_{R1}$	6.16	5.10	5.13	5.15	5.13	5.10
$f(\nu C\text{-}H)_{R2}$	5.31	5.29	5.29	5.32	5.29	5.10
$f(\nu C\text{-}H)_{R3}$	5.15	5.16				
$f(\nu C\text{-}N)_{Chain}$	7.36	7.80	9.46	9.27	7.46	6.10
$f(\nu C\text{-}N)_R$	6.64	6.54	6.74	6.61	6.74	4.32
$f(\nu N\text{-}N)_R$	5.99	6.02	5.86	5.97	5.85	3.90
$f(\nu N\text{-}N)_{Chain}$	5.75	5.34	5.64	5.31	5.56	6.73
$f(\nu C{=}C)_{R1}$	6.34	6.31	6.31	6.27	6.24	6.15
$f(\nu C{=}C)_{R2}$	6.15	6.23	6.84	6.80	6.84	7.31
$f(\nu C{=}C)_{R3}$	6.34	6.35				

Units are mdyn Å^{-1} for stretching and mdyn Å rad^{-2} for angle deformations.

[a] This work

[b] From Ref [18] for (*E*)-*N*'-4-methoxybenzylidene)-5-methyl-*1H*-pyrazole-3-carbohydrazide (E-MBPC)

[c] From Ref [19] for (*E*)-*N*'-(4-(dimethylamino)benzylidene)-5-methyl-*1H*-pyrazole-3-carbohydrazide[b](E-MABPC).

3.8. ^{1}H-NMR analysis

The proton NMR spectrum of E-DPPC was obtained by using TMS as an internal standard and DMSO-d_6 as solvent (**Fig. S13**). The ^{1}H-NMR spectra of the title molecule displayed a singlet at δ = 7.24 ppm due to proton H28 of pyrazole ring. The chemical shifts of aromatic protons (H5, H34 and H36) appeared as multiplet between δ = 7.52 and 7.34 ppm, and the chemical shifts of H8, H3 and H30 appeared as three doublets at δ = 7.69, 7.82 and 8.01 ppm, respectively, and. The chemical shifts of the azomethine (N=CH) and amide (NHCO) protons (H23 and H13) appear as a singlet at δ = 8.89 and 12.12 ppm, respectively. The chemical shifts of NH pyrazole (H21) appeared as singlet at δ = 13.83 ppm. Comparisons between experimental and calculated ^{1}H chemical shifts for E-DPPC in aqueous solution by using B3LYP/6-311++G** calculation and the GIAO method [51] are presented in **Table S6** by using the RMSD values. Reasonable correlations are obtained for the H atoms with a RMSD value of 1.62 ppm. The ^{13}C NMR spectrum in aqueous solution was also predicted at the same level of theory with the GIAO method but the comparisons with the experimental values were no presented due to a very bad quality of experimental NMR spectrum. For this reason, in **Table S7** are presented only the predicted ^{13}C-NMR chemical shifts.

3.9. Electronic spectrum

The ultraviolet-visible spectrum of **E-DPPC** was obtained in methanol and it is compared in **Fig. S14** with the corresponding predicted in aqueous solution by using B3LYP/6-311++G** calculation. In the experimental spectrum of **E-DPPC** are observed two maxima at 273 and 280 nm and a less intense and broad band at c.a. 310 nm while in the predicted spectrum are observed two bands a lees intense at 265 nm and other of higher intensity at 308 nm. Here, the less intense band observed at 265 nm in the theoretical spectrum could overlap those two intense bands at 273 and 280 nm while the other band is predicted with higher intensity. Evidently, the presence of C=C double bonds of both dichlorobenzylidene and phenyl rings suggest that the most intense bands could be associated to $\pi \rightarrow \pi^*$ transitions while the other band of lower intensity can be attributed to $n \rightarrow \pi^*$ and $\pi^* \rightarrow \pi^*$ transitions, as suported by NBO calculations. These assignments are in agreement with compounds containing similar groups [18,19,59–61].

3.10. ESI-MS study

The ESI-MS spectra show molecular ion peaks with m/z values 359.0 correspond to the molecular weight $[M+H]^+$. The m/z value 381.0 correspond to the sodiated molecular ion peak $[M+Na]^+$ (**Fig. S15**). These values are in good agreement with the proposed composition for the title molecule ($C_{17}H_{12}Cl_2N_4O$).

3.11. Molecular docking analysis

3.11.1. Binding energy evaluation of synthesized compound

To predict the best conformational position within the active region of target protein, the ligand (**E-DPPC**) was docked against caspase-3. Docking results justified that ligand possessed good binding energy value (-8.30 Kcal/mol) and good interactive behavior. The other poses also showed good energy values as mentioned in supplementary data (**Table S8**).

3.11.2. Binding pocket analysis

The ligand structure binds at opening region of binding pocket. The ligand structure is little bulky molecule having couple of halogen atoms at one side whereas other part contain benzene ring structure. The benzene ring having chlorine atoms showed its presence at opening region of binding pocket, whereas the benzene ring showed its presence outside the opening side of binding pocket. The graphical representation of binding pocket is represented in Fig. 5.

3.11.3. Binding interaction behavior

The best docked complex was selected to better understand the binding interaction behavior of ligand (**E-DPPC**) against caspase-3. Docking analysis showed that compound **E-DPPC** was actively confined within active binding region of receptor molecule (Fig. 4 **A**). In detail, the structure activity relationship (SAR) study showed that one hydrogen and one hydrophobic interaction was observed in **E-DPPC**-docking complex. The nitrogen atom of five membered ring structure in **E-DPPC** forms single hydrogen bond with Lys137 having bond length 2.90 Å. Moreover, chlorine (Cl) atom of **E-DPPC** forms hydrophobic interaction with bond length 3.70 Å against Val266. Research data also ensured the importance of these residues in bonding with other caspase-3 inhibitors which strengthen our docking results [62]. The computational binding energy and SAR analysis showed the significance of **E-DPPC** and may consider as potent inhibitor against caspase-3 (Fig. 4 **B**).

4. Conclusions

Here, the new *(E)-N'*-(2,4-dichlorobenzylidene)-5-phenyl-*1H*-pyrazole-3-carbohydrazide (**E-DPPC**) has been synthesized and characterized by using FT-IR, ^{1}H-NMR, ESI-MS, and single-crystal X-ray diffraction. Functional hybrid B3LYP/6-311++G** calculations were performed in gas phase and in aqueous solution to study the structures and properties of this new pyrazole-3-carbohydrazide derivative. In solution, the calculations were carried out with the self-consistent reaction field (SCRF) method and, the IEFPCM and universal solvation models. Two stable structures with similar energies were found in the PES and, for these reasons, only the properties of conformer C2 were studied in both media. C2 evidence a higher dipole moment and a volume contraction in solution attributed to the presence of two donors H bonds groups (N-H) and of five acceptors H bonds (N and O atoms). Besides, the changes in orientation and direction of dipole moment vector in solution are attributed to the hydration of **E-DPPC** with water molecules. C2 shows a ΔG_c value of -130.83 kJ/mol between *(E)-N'*-4-methoxybenzylidene)-5-methyl-*1H*-pyrazole-3-carbohydrazide (E-MBPC) (-131.34 kJ/mol) and *(E)-N'*-(4-(dimethylamino)benzylidene)-5-methyl-*1H*-pyrazole-3-carbohydrazide (E-MABPC) (-129.50 kJ/mol) derivatives. The repulsion existent between the negative MK, Mulliken and NPA charges on the N12 and O15 atoms explain the diminishing of N12-C14-O15 angle from 123.77 ° in gas phase to 123.03 ° in solution.

Nucleophilic sites are visibly observed on the acceptor H bonds groups (N10, O15 and N22 atoms) while on the N18-H21, N12-H13, C11-H23, C2-H3, C17-H20 bonds characteristics electrophilic sites donors H bonds, being the N18-H21 bond the most labile donor of H bond with the lowest MEP and bond order values. NBO calculations suggest that C2 in aqueous solution is clearly most stable than in gas phase. AIM studies show that C2 of **E-DPPC** is stable in both media due to new H bonds formed. The gap value in solution (4.3294 eV) has a lower value than that observed in gas phase (4.3674 eV) indicating this way, that C2 is most reactive in solution. The harmonic force fields in both media were calculated together with the scaled force constants while the 102 vibration normal modes expected for C2 were completely assigned. The comparisons of experimental NMR and UV-visible spectra with the corresponding predicted evidence reasonable correlations. Additionally, the molecular docking results ascertained the binding relationship between the **E-DPPC** and enzyme. Thus, it can be indicated that,

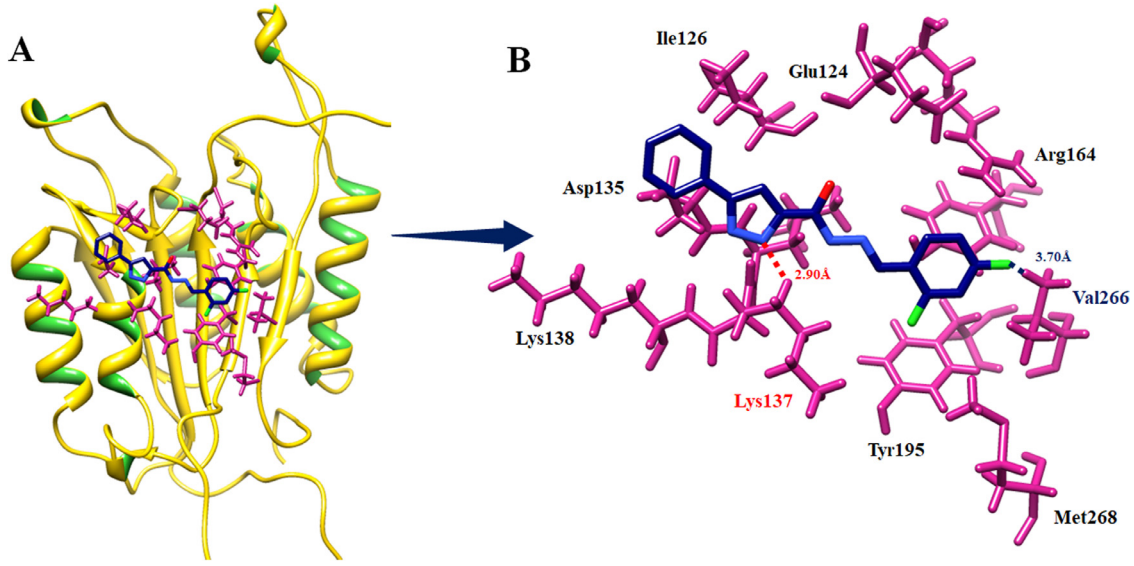

Fig. 4. Binding pocket of target protein.

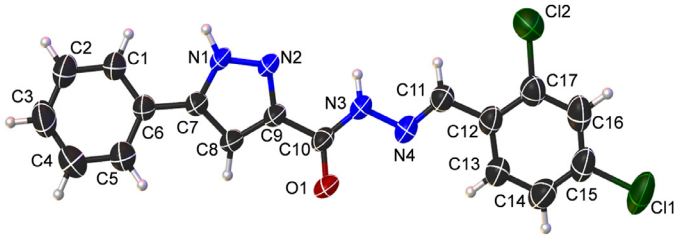

Fig. 5. (A, B). Binding pocket of caspase-3 with **E-DPPC** interaction. The binding pocket residues are highlighted in purple color while ligand structure is represented in blue color. The hydrogen and hydrophobic interaction are labelled with red and dark blue colors, having distances mentioned in angstrom (Å).

E-DPPC could be exploited as a potent aspirant of the drug by targeting caspase-3 in medicinal field.

5. Credit Author Statement

Khalid Karrouchi: Conceptualization, Methodology, Original Draft, Writing - Review & Editing.

Silvia A. Brandán : Software, Validation, Writing- Reviewing and Editing.

Mubashir Hassan: Software, Molecular docking, Writing - Original Draft.

Khalid Bougrin: Investigation.

Smaail Radi: Supervision, Project administration.

Marilena Ferbinteanu: Software, Validation, Writing - Review.

Yann Garcia: Supervision, Investigation.

M'hammed Ansar: Supervision, Project administration.

Declaration of Competing Interest

All authors declare that there are no conflicts of interest.

Acknowledgments

This work was supported by the WBI-COP22 Morocco project and UM5R as well as grants from CIUNT Project N° 26/D608 (Consejo de Investigaciones, Universidad Nacional de Tucumán). The authors would like to thank Prof. Tom Sundius for his permission to use MOLVIB.

Supplementary materials

Supplementary material associated with this article can be found, in the online version, at doi:10.1016/j.molstruc.2020.129714.

References

[1] K. Karrouchi, S. Radi, Y. Ramli, J. Taoufik, Y. Mabkhot, F. Al-aizari, M. Ansar, Synthesis and pharmacological activities of pyrazole derivatives: a review, Molecules 23 (2018) 134.

[2] F.E. Bennani, L. Doudach, Y. Cherrah, Y. Ramli, K. Karrouchi, M. Ansar, M.E.A. Faouzi, Overview of recent developments of pyrazole derivatives as an anticancer agent in different cell line, Bioorg. Chem (2019) 103470.

[3] K. Karrouchi, S. Fettach, S. Radi, J. Taoufik, Y.N. Mabkhot, S. Alterary, My E.A Faouzi, M. Ansar, Synthesis, Characterization, Free-radical Scavenging Capacity and Antioxidant Activity of Novel Series of Hydrazone, 1, 3, 4-oxadiazole and 1, 2, 4-triazole Derived from 3, 5-dimethyl-1H-pyrazole, Lett. Drug. Des. Discov. 16 (2019) 712–720.

[4] A. Titi, M. Messali, B.A. Alqurashy, R. Touzani, T. Shiga, H. Oshio, T.B. Hadda, Synthesis, characterization, X-Ray crystal study and bioctivities of pyrazole derivatives: Identification of antitumor, antifungal and antibacterial pharmacophore sites, J. Mol. Struct. 1205 (2020) 127625.

[5] K. Karrouchi, E.B. Yousfi, N.K. Sebbar, Y. Ramli, J. Taoufik, Y. Ouzidan, M. Ansar, Y.N. Mabkhot, H.A. Ghabbour, S. Radi, New Pyrazole-Hydrazone Derivatives: X-ray Analysis, Molecular Structure Investigation via Density Functional Theory (DFT) and Their High In-Situ Catecholase Activity, Int. J. Mol. Sci. 18 (2017) 2215.

[6] A.T. Taher, M.T.M. Sarg, N.R.E.S. Ali, N.H. Elnagdi, Design, synthesis, modeling studies and biological screening of novel pyrazole derivatives as potential analgesic and anti-inflammatory agents, Bioorg. chem. 89 (2019) 103023.

[7] S. Tighadouini, R. Benabbes, M. Tillard, D. Eddike, K. Haboubi, K. Karrouchi, S. Radi, Synthesis, crystal structure, DFT studies and biological activity of (Z)-3-(3-bromophenyl)-1-(1, 5-dimethyl-1 H-pyrazol-3-yl)-3-hydroxyprop-2-en-1-one, Chem. Cent. J. 12 (1) (2018) 122.

[8] Y. Xu, Z. Zhang, X. Jiang, X. Chen, Z. Wang, H. Alsulami, W. Tang, Discovery of δ-sultone-fused pyrazoles for treating Alzheimer's disease: Design, synthesis, biological evaluation and SAR studies, Eur. J. Med. Chem. 181 (2019) 111598.

[9] K. Karrouchi, L. Chemlal, J. Taoufik, Y. Cherrah, S. Radi, M-E. Faouzi, M. Ansar, Synthesis, antioxidant and analgesic activities of Schiff bases of 4-amino-1, 2, 4-triazole derivatives containing a pyrazole moiety, Ann. Pharm. Fr. 74 (2016) 431–438.

[10] K. Chkirate, S. Fettach, K. Karrouchi, N.K. Sebbar, E.M. Essassi, J.T. Mague, S. Radi, M.E.A. Faouzi, N.N. Adarsh, Y Garcia, Novel Co (II) and Cu (II) coordination complexes constructed from pyrazole-acetamide: Effect of hydrogen bonding on the self assembly process and antioxidant activity, J. Inorg. Biochem. 191 (2019) 21–28.

[11] R.R. Pillai, K. Karrouchi, S. Fettach, S. Armaković, S.J. Armaković, Y. Brik, J. Taoufik, S. Radi, M.E.A. Faouzi, M.H. Ansar, Synthesis, spectroscopic characterization, reactive properties by DFT calculations, molecular dynamics simulations and biological evaluation of Schiff bases tethered 1, 2, 4-triazole and pyrazole rings, J. Mol. Struct. 1177 (2019) 47–54.

[12] H. Dai, Y.-S. Xiao, Z. Li, X.-Y. Xu, X.-H. Qian. Dai, H., Xiao, Y. S., Li, Z., Xu, X. Y., & Qian, X. H. The thiazoylmethoxy modification on pyrazole oximes: Synthe-

sis and insecticidal biological evaluation beyond acaricidal activity. Chinese Chemical Letters, 25(7), 1014-1016.
[13] K. Korber, F. Kaiser, G. Veitch, W. Von Deyn, N. G. Bandur, J. Dickhaut, K. Gunjima. U.S. Patent No. 9,174,967. Washington, DC: U.S. Patent and Trademark Office, (2015).
[14] Y.C. Lang, Y.L. Bai, Research and development progresses on pyrazole agrochemicals, Modern Agrochemicals. 5 (2006) 6.
[15] L.R.S. Dias, R.R.S. Salvador, Pyrazole Carbohydrazide Derivatives of Pharmaceutical Interest, Pharmaceuticals 5 (2012) 317–324.
[16] S. Rollas, S.G. Küçükgüzel, Biological activities of hydrazone derivatives, Molecules 12 (2007) 1910–1939.
[17] C. Sivakumar, V. Balachandran, B. Narayana, V.V. Salian, B. Revathi, N. Shanmugapriya, K. Vanasundari, Molecular spectroscopic assembly of 3-(4-chlorophenyl)-5-[4-(propane-2-yl) phenyl] 4, 5-dihydro-*1H*-pyrazole-1-carbothioamide, antimicrobial potential and molecular docking analysis, J. Mol. Struct. (2020) 128005.
[18] K. Karrouchi, S.A. Brandán, Y. Sert, H. El-marzouqi, S. Radi, M. Ferbinteanu, M.E.A. Faouzi, Y. Garcia, M. Ansar, Synthesis, X-ray structure, Vibrational spectroscopy, DFT investigation and biological evaluation studies of (*E*)-*N*'-(4-(dimethylamino)benzylidene)-5-methyl-1H-pyrazole-3-carbohydrazide, J. Mol. Struct. 1219 (2020) 128541.
[19] K. Karrouchi, S.A. Brandán, Y. Sert, M. El Karbane, S. Radi, M. Ferbinteanu, Y. Garcia, M. Ansar, Synthesis, structural, molecular docking and spectroscopic studies of (E)-N'-(4-methoxybenzylidene)-5-methyl-1H-pyrazole-3-carbohydrazide, submitted to J. Mol. Struct. (2020).
[20] S. Özkınalı, M. Gür, N. Şener, S. Alkın, M.S. Çavuş, Synthesis of new azo schiff bases of pyrazole derivatives and their spectroscopic and theoretical investigations, J. Mol. Struct. 1174 (2018) 74–83.
[21] Y. Bouzian, K. Karrouchi, Y. Sert, C.H. Lai, L. Mahi, N.H. Ahabchane, A. Talbaoui, J. T. Mague, E. M. Essassi. Synthesis, spectroscopic characterization, crystal structure, DFT, molecular docking and in vitro antibacterial potential of novel quinoline derivatives, J. Mol. Struct. 1209 (2020) 127940.
[22] J. Kausteklis, V. Aleksa, M.A. Iramain, S.A. Brandán, Cation-anion interactions in 1-buthyl-3-methyl imidazolium nitrate ionic liquid and their effect on their structural and vibrational properties, J, Mol. Struct. 1164 (2018) 1–14.
[23] O. Noureddine, S. Gatfaoui, S.A. Brandán, H. Marouani, N. Issaoui, Structural, docking and spectroscopic studies of a new piperazine derivative, 1-Phenylpiperazine-1,4-diium-bis (hydrogen sulfate), J Mol. Struct. 1202 (2020) 127351.
[24] S. Gatfaoui, N. Issaoui, S.A. Brandán, T. Roisnel, H. Marouani, Synthesis and characterization of p-xylylenediaminiumbis(nitrate). Effects of the coordination modes of nitrate groups on their structural and vibrational properties, J. Mol. Struct. 1151 (2018) 152–168.
[25] O. Noureddine, S. Gatfaoui, S.A. Brandan, A. Sagaama, H. Marouani, N. Issaoui, Experimental and DFT studies on the molecular structure, spectroscopic properties, and molecular docking of 4-phenylpiperazine-1-ium dihydrogen phosphate, J Mol. Struct. 1207 (2020) 127762.
[26] M.A. Iramain, A.E. Ledesma, E. Imbarack, P.L. Bongiorno, S.A. Brandán, Spectroscopic studies on the potassium 1-fluorobenzoyltrifluoroborate salt by using the FT-IR, Raman and UV–Visible spectra and DFT calculations, J. Mol. Struct. 1204 (2020) 127534.
[27] K. Karrouchi, S. Fettach, Mukesh M. Jotani, A. Sagaama, S. Radi, H.A. Ghabbour, Y.N. Mabkhot, B. Himmi, M.E.A. Faouzi, N. Issaoui, Synthesis, crystal structure, hirshfeld surface analysis, DFT calculations, anti-diabetic activity and molecular docking studies of (E)-N'-(5-bromo-2-hydroxybenzylidene) isonicotinohydrazide, J. Mol. Struct. (2020) 128800.
[28] P. Pulay, G. Fogarasi, G. Pongor, J.E. Boggs, A. Vargha, Combination of theoretical ab initio and experimental information to obtain reliable harmonic force constants. Scaled quantum mechanical (QM) force fields for glyoxal, acrolein, butadiene, formaldehyde, and ethylene, J. Am. Chem. Soc. 105 (1983) 7073.
[29] T. Sundius, Scaling of ab-initio force fields by MOLVIB, Vib. Spectrosc. 29 (2002) 89–95.
[30] G. Rauhut, P. Pulay, Transferable Scaling Factors for Density Functional Derived Vibrational Force Fields, J. Phys. Chem. 99 (1995) 3093–3100.
[31] K. Karrouchi, M. Ansar, S. Radi, M. Saadi, L. El Ammari, Crystal structure of N′-diphenylmethylidene-5-methyl-1H-pyrazole-3-carbohydrazide, Acta Cryst E 71 (2015) o890–o891.
[32] K. Karrouchi, S. Radi, J. Taoufik, H.A. Ghabbour, Y.N. Mabkhot, Crystal structure of N′-(4-(dimethylamino) benzylidene)-5-phenyl-1H-pyrazole-3-carbohydrazide, C19H19N5O, Z. Kristallogr. NCS 231 (2016) 883–886.
[33] K. Karrouchi, S. Radi, J. Taoufik, H.A. Ghabbour, Y.N. Mabkhot, Crystal structure of N′-(4-methoxybenzylidene)-5-phenyl-1H-pyrazole-3-carbohydrazide, C18H16N4O2, Z. Kristallogr. NCS. 231 (2016) 835–837.
[34] K. Karrouchi, S. Radi, J. Taoufik, H.A. Ghabbour, Y.N. Mabkhot, Crystal structure of N′-(4-nitrobenzylidene)-5-phenyl-1H-pyrazole-3-carbohydrazide, C17H13N5O3, Z. Kristallogr. NCS 231 (2016) 839–841.
[35] Crystal Structure 4.2: Crystal Structure Analysis Package, Rigaku Corporation (2000-2015). Tokyo, Japan.
[36] O.V. Dolomanov, L.J. Bourhis, R.J. Gildea, J.A.K. Howard, H. Puschmann, OLEX2: A complete structure solution, refinement and analysis program, J. Appl. Cryst. 42 (2009) 339–341.
[37] G.M. Sheldrick, Acta Crystallogr., Sect. C: Struct. Chem. 71 (2015) 3–8.
[38] C.F. Macrae, P.R. Edgington, P. McCabe, E. Pidcock, G.P. Shields, R. Taylor, M. Towler, J. Van De Streek, Mercury: visualization and analysis of crystal structures, J. Appl. Crystallogr. 39 (2006) 453–457.
[390] G.M. Sheldrick, Crystal structure refinement with SHELXL, Acta Cryst C. (2015) 71.
[40] M.J. Frisch, G. W. Trucks, H.B. Schlegel, G.E. Scuseria, M.A. Robb, J.R. Cheeseman, G. Scalmani, V. Barone, B. Mennucci, G.A. Petersson, H. Nakatsuji, M. Caricato, X. Li, H.P. Hratchian, A.F. Izmaylov, J. Bloino, G. Zheng, J.L. Sonnenberg, M. Hada, M. Ehara, K. Toyota, R. Fukuda, J. Hasegawa, M. Ishida, T. Nakajima, Y. Honda, O. Kitao, H. Nakai, T. Vreven, J.A. Montgomery, Jr, J.E. Peralta, F. Ogliaro, M. Bearpark, J.J. Heyd, E. Brothers, K. N. Kudin, V.N. Staroverov, R. Kobayashi, J. Normand, K. Raghavachari, A. Rendell, J.C. Burant, S.S. Iyengar, J. Tomasi, M. Cossi, N. Rega, J.M. Millam, M. Klene, J.E. Knox, J.B. Cross, V. Bakken, C. Adamo, J. Jaramillo, R. Gomperts, R.E. Stratmann, O. Yazyev, A.J. Austin, R. Cammi, C. Pomelli, J.W. Ochterski, R.L. Martin, K. Morokuma, V.G. Zakrzewski, G.A. Voth, P. Salvador, J.J. Dannenberg, S. Dapprich, A.D. Daniels, O. Farkas, J.B. Foresman, J.V. Ortiz, J. Cioslowski, and D.J. Fox, Gaussian, Inc., Wallingford CT, 2009.
[41] A.D. Becke, Density-functional exchange-energy approximation with correct asymptotic behavior, Phys. Rev. 38 (1988) 3098–3100.
[42] C. Lee, W. Yang, R.G. Parr, Development of the Colle-Salvetti correlation-energy formula into a functional of the electron density, Phys. Rev. 37 (1988) 785–789.
[43] E.D. Glendening, J.K. Badenhoop, A.D. Reed, J.E. Carpenter, F. Weinhold, NBO 3.1, Theoretical Chemistry Institute, University of Wisconsin, Madison, WI, 1996.
[44] R.F.W. Bader, Atoms in Molecules, A Quantum Theory, Oxford University Press, Oxford, 1990 , ISBN: 0198558651.
[45] F. Biegler-Köning, J. Schönbohm, D. Bayles, AIM2000; A Program to Analyze and Visualize Atoms in Molecules, J. Comput. Chem. 22 (2001) 545.
[46] B.H. Besler, K.M. Merz Jr, P.A. Kollman, Atomic charges derived from semiempirical methods, J, Comp. Chem. 11 (1990) 431–439.
[47] A.B. Nielsen, A.J. Holder, Gauss View 5.0, User's Reference, GAUSSIAN Inc., Pittsburgh, PA, 2008.
[48] R.G. Parr, R.G. Pearson, Absolute hardness: companion parameter to absolute electronegativity, J, Am. Chem. Soc. 105 (1983) 7512–7516.
[49] G. Keresztury, S. Holly, G. Besenyei, J. Varga, A.Y. Wang, J.R. Durig, Vibrational spectra of monothiocarbamates-II. IR and Raman spectra, vibrational assignment, conformational analysis and ab initio calculations of S-methyl-N,N-dimethylthiocarbamate, Spectrochim. Acta 49A (1993) 2007–2026.
[50] D. Michalska, R. Wysokinski, The prediction of Raman spectra of platinum(II) anticancer drugs by density functional theory, Chemical Physics Letters 403 (2005) 211–217.
[51] R. Ditchfield, Self-consistent perturbation theory of diamagnetism. I. A gage-invariant LCAO (linear combination of atomic orbitals) method for NMR chemical shifts, Mol Phys 27 (1974) 714–722.
[52] S. Miertus, E. Scrocco, J. Tomasi, Electrostatic interaction of a solute with a continuum, Chem. Phys. 55 (1981) 117–129.
[53] J. Tomasi, J. Persico, Molecular Interactions in Solution: An Overview of Methods Based on Continous Distributions of the Solvent, Chem. Rev. 94 (1994) 2027–2094.
[54] A.V. Marenich, C.J. Cramer, D.G. Truhlar, Universal solvation model based on solute electron density and a continuum model of the solvent defined by the bulk dielectric constant and atomic surface tensions, J. Phys. Chem. 113 (2009) 6378–6396.
[55] P. Ugliengo, MOLDRAW Program, University of Torino, Dipartimento Chimica IFM, Torino, Italy, 1998.
[56] EF Pettersen, TD Goddard, CC Huang, GS Couch, DM Greenblatt, et al., UCSF Chimera–a visualization system for exploratory research and analysis, J Comput Chem 25 (2004) 1605–1612.
[57] D Studio, Discovery. "version 2.1.", Accelrys, San Diego, CA, 2008.
[58] S Dallakyan, AJ Olson, Small-molecule library screening by docking with PyRx, Methods Mol Biol 1263 (2015) 243–250.
[59] M Minteguiaga, E Dellacassa, MA Iramain, CAN Catalán, SA Brandán, FT-Raman FT-IR, NMR and structural studies of Carquejyl Acetate, a component of the essential oil from *Baccharis trimera* (Less.) DC. (Asteraceae), submitted to J Mol. Struct 1177 (2019) 499–510.
[60] T.J. Bruno, P.D.N. Svoronos, CRC Handbook of Basic Tables for Chemical Analysis, Second Edition, CRC Press, Taylor & Francis Goup, Boca Raton, 2011.
[61] J. Ruiz Hidalgo, A. Neske, M.A Iramain, P.E. Alvarez, P. Leyton Bongiorno, S.A. Brandán, FT-IR, FT-Raman and UV-visible spectra of motrilin acetogenin isolated from *Annona cherimolia*, J Mol. Struct. 1196 (2019) 508–517.
[62] Y.E. Hadisaputri, N. Cahyana, M. Muchtaridi, R. Lesmana, T. Rusdiana, A.Y. Chaerunisa, I. Sufiawati, T. Rostinawati, A. Subarnas, Apoptosis-mediated antiproliferation of A549 lung cancer cells mediated by Eugenia aquea leaf compound 2′,4′-dihydroxy-6′-methoxy-3′,5′-dimethylchalcone and its molecular interaction with caspase receptor in molecular docking simulation, Oncology letters 19 (2020) 3551–3557.